Mechanistic Deep Learning Framework on Cell Traits Derived from Single-Cell Mass Cytometry Data

Bo Wang[1], Sandra S. Zinkel[2,3], and Eric R. Gamazon[1, 4, 5, 6]

[1]Division of Genetic Medicine, Department of Medicine, Vanderbilt University Medical Center, Nashville, TN, USA

[2]Department of Cell and Developmental Biology, Vanderbilt University, Nashville, TN, USA

[3]Department of Medicine, Vanderbilt University Medical Center, Nashville, TN, USA

[4]Vanderbit Genetics Institute, Vanderbilt University Medical Center, Nashville, TN, USA

[5]Data Science Institute, Vanderbilt University Medical Center, Nashville, TN

[6]Clare Hall, University of Cambridge, Cambridge, United Kingdom

Send correspondence to:

Eric R. Gamazon <eric.gamazon@vumc.org> or Sandra Zinkel <sandra.zinkel@vumc.org>

Abstract

Germline genetic variations can alter cellular differentiation, potentially impacting the response of immune cells to inflammatory challenges. Current variant- and gene- based methods in mouse and human models have established associations with disease phenotypes; however, the underlying mechanisms at the cellular level are less well-understood. Immunophenotyping by multi-parameter flow cytometry, and more recently mass cytometry, has allowed high-resolution identification and characterization of hematopoietic cells. The obtained characterization yields increased dimensionality; however, conventional analysis workflows have been inefficient, incomplete, or unreliable. In this work, we develop a comprehensive machine learning framework – MDL4Cyto – that is tailored to the analysis of mass cytometry data, incorporating statistical, unsupervised learning, and supervised learning models. The statistical modeling can be used to illuminate cell fate decision and cell-type dynamics. The unsupervised learning models along with complementary marker enrichment analyses highlight genetic perturbations that are significantly associated with alterations in cell populations in the hematopoietic system. Furthermore, our supervised learning models, including deep learning and tree-based algorithms, address the bottleneck to data pre-processing that characterizes conventional workflows and generate inferences (e.g., on marker/cell-type interactions) from raw experimental characterization. Notably, we reveal a close relationship among network design, prediction performance, and the underlying biological context. We show that the network architecture extracted from the differentiation cascade of the investigated biological system yields enhanced prediction performance. The presented methodology will enable new insights into hematopoietic differentiation at baseline and following perturbation.

Highlights

- Analysis pipeline on mass cytometry data with high-performance implementation of statistical, unsupervised learning, and supervised learning models
- Concordance of machine learning results with biological contexts
- Biologically-informed neural network designs enhance prediction performance

Graphical Abstract

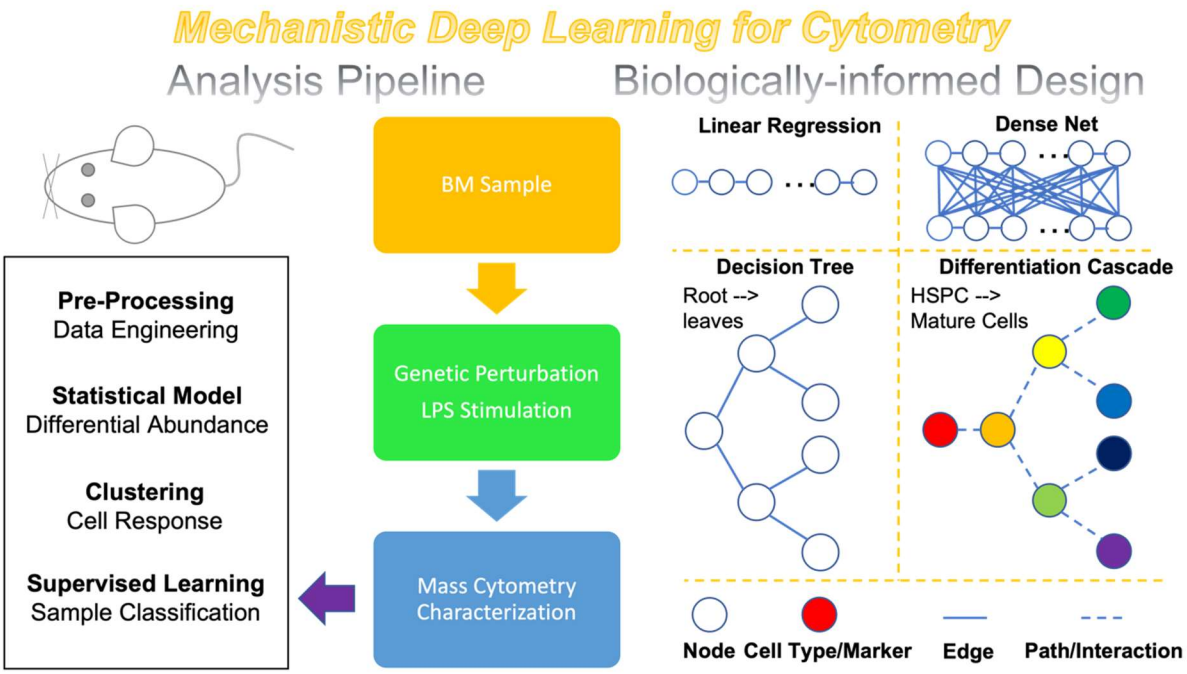

Keywords

Machine Learning, Mass Cytometry, CyTOF, Hematopoiesis, Cellular Differentiation, Regulatory Cascade, Clonal Hematopoiesis of Indeterminate Potential

Introduction

Hematopoiesis is a hierarchical and dynamic process. Proper blood cell development requires highly coordinated and tightly regulated cytokine signals, affecting cell and stage-appropriate gene expression. Genetically modified mouse models are an invaluable model system for studying hematopoiesis, due to their defined genetic background, wealth of reagents to precisely define hematopoietic cell populations, ability to undergo precise genetic modification, and the wealth of data and assays arising from decades of study. Cytometry tools have proved to be essential in simultaneously analyzing labeled molecules at the single-cell level and, consequently, have been widely implemented in basic and clinical research[1]. While traditional fluorescence cytometers can detect up to 35 markers, the technique is limited by spectral overlap of fluorophores. Single-cell mass cytometry (Cytometry by Time-Of-Flight [CyTOF]) enables multiple-parameter tracking by the use of metal-isotope-tagged antibodies, overcoming the inherent limitations of spectral overlap. Therefore, a more comprehensive panel of cellular functions (achieved from significantly expanded feature capacity[2]) along with intracellular signaling states can be explored to identify disease-associated changes or functionally-relevant states; differential expression under external perturbation or intracellular response is more easily elucidated[3].

Insights from cytometry characterization are traditionally extracted from manual gating. Automated workflows such as FlowCore[4], PhenoGraph[5] or the recently reported Tracking Responders EXpanding (T-REX)[6] have been introduced with significantly enhanced processing efficiency. However, these pipelines are still limited by expert intervention into (manual) data pre-processing, where key thresholds for transformation, gating or cell type clustering are tailored to the investigated systems. Recently, machine learning algorithms have attracted significant attention for their extensive application to the analysis of cytometry data[6–8]. Specifically, beyond functioning as embedded algorithms in pipelines, machine learning tools provide “end-to-end” solutions, generating inferences or predictions

78 directly from raw experimental characterization, with potential to uncover novel associations that are
79 obscured by conventional gating strategies.

80 Hematopoiesis has served as a paradigm of stem cell biology[9]. Genetic perturbations within cells
81 (in particular, Hematopoietic Stem and Progenitor Cell [HSPC]) induce challenges to cellular functions,
82 thus leading to various diseases or conditions, e.g., Clonal Hematopoiesis of Indeterminate Potential
83 (CHIP), Myelodysplastic Syndromes (MDS), and Acute Myeloid Leukemia (AML). Tet2 inactivating
84 mutations are among the early mutations that initiate clonal expansion (CHIP). As the most expressed
85 Tet gene in the hematopoietic tissue (especially in HSCs), Tet2 functions as a tumor suppressor whose
86 haplo-insufficiency initiates myeloid and lymphoid transformations[8]. Tet2 has been shown to regulate
87 resolution of inflammatory responses. Tet2 KO mice and cell lines display prolonged and enhanced
88 inflammatory cytokine signaling, which impacts HSPC differentiation.

89 Hematopoietic homeostasis is further controlled through tight regulation of programmed cell
90 death. The two major types of cell death, apoptosis (programmed cell death) and necrosis (uncontrolled
91 cell death), maintain homeostasis by downregulating detrimental inflammation and prevent
92 transformation by allowing efficient removal of damaged cells. It has been widely recognized that the
93 genes in the Bcl-2 family are critical in regulating apoptosis[10,11], comprising of both pro-survival
94 members and pro-apoptotic members. The functions of BID (pro-apoptotic member and multidomain
95 effector) were investigated and confirmed in our previous genomic studies[12]. Specifically, an association
96 between decreased genetically determined BID expression and myocardial infarction susceptibility was
97 identified in a discovery cohort using a gene-based association method[13], and validated by two
98 independent genome-wide association studies (GWAS). In the follow-up studies, we further tested the
99 functionalities of proteins in the family, including multidomain effectors Bax, Bak and the BH3-only
100 protein, Bid, in murine models[14]. We found that deletion of Bax/Bak inhibits both bone marrow
101 apoptosis and bone marrow necroptosis. Further deletion of BH3-only member Bid (TKO) leads to robust

activation of necroptosis, which results in a phenotype characterized by dysplasia and cytopenia, resembling the bone marrow failure disorder MDS (myelodysplastic syndrome)[14].

To address the limitations of conventional cytometry data analysis pipelines[5–8,15], we developed a comprehensive *Mechanistic Deep Learning for Cytometry* (MDL4Cyto) framework, implementing statistical, unsupervised learning, and supervised learning models. The framework was evaluated against bone marrow samples of murine models that have been genetically perturbed in the hematopoietic system, including Wild Type (WT), *VavCreBaxBakBid* triple-knockout (TKO), and *VavCreTet2* knock-out (Tet2 KO) mice, and validated with biological observations. Notably, building on our previous work[16,17], we designed the architectures of the neural networks using the intrinsic hierarchy of the hematopoietic system as a guide, establishing a *biological feature – network architecture – phenotype* relationship. We show that biologically-informed network designs could function as probes on the regulatory cascade with prediction performance as the evaluation metric. Our framework may inform future machine learning implementations to address fundamental questions in cell biology.

Results

Overview of mass cytometry data and MDL4Cyto framework

Mice from three genetic murine models – WT, Tet2 and TKO – were treated with Phosphate-buffered saline (PBS) or lipopolysaccharide (LPS). LPS is a major surface membrane polysaccharide found on Gram-negative bacteria and is a typical pathogen-associated molecular pattern (PAMP). Inflammation triggered by LPS stimulation activates a robust innate immune response and can induce the proliferation of hematopoietic progenitor cells[18] and the production of cytokines such as TNFα, interleukin and IL-2. Bone marrow from these mice was subsequently harvested and processed for

124 cytometry experiments. Besides genetic perturbations, all the samples challenged by LPS stimulation
125 were compared to the PBS vehicle control (Figure 1A). Across different types of samples (WT-PBS, WT-
126 LPS, Tet2-PBS, Tet2-LPS, TKO-PBS, and TKO-LPS), lineage marker groups (Stem Cells, Pan Leukocyte
127 Markers, T Lymphocytes, Mature Myeloid Cells, B cells, and Erythrocytes) and functional marker groups
128 (Cytokines, Cell death and Proliferation), were tagged and monitored (Table S1). As sample data profiles
129 obtained from the mass cytometry measurements varied in length, we imputed data points at each of
130 the six sample data profiles via binning methods with 30 seconds.

131 We developed MDL4Cyto, an analysis pipeline for mass cytometry data (Figure 1B and
132 **Methods**), implementing statistical, unsupervised, and supervised learning models. Statistical tests on
133 the cell count of key lineage and functional markers were performed, aiming for a glimpse of the
134 underlying biology. As both genetic perturbations and LPS stimulation may induce inflammatory changes
135 in hematopoiesis, we applied Generalized Mixed-Effects Model (GMM) estimation to determine the
136 extent to which cell count was statistically altered by these modifications. Two established workflows,
137 namely PhenoGraph[5] and T-REX[6], were benchmarked as established pipelines capable of annotating cell
138 populations or capturing cell responses. In addition, supervised learning models were explicitly designed
139 to probe marker/cell-type interactions within the regulatory cascade, as well as to predict sample type
140 directly from the raw mass cytometry characterization. Nine machine learning models were evaluated,
141 including Linear Regression (LR), Dense Neural Network (DNN), Boosted Tree (BT), Random Forest (RF),
142 stacked Dense Neural Network - Random Forest (DNN-RF), Convolutional Neural Network in One
143 Dimension (CNN-1D), Convolutional Neural Network in Two Dimensions (CNN-2D), Recurrent Neural
144 Network with Long Short-Term Memory cell (RNN-LSTM), and Recurrent Neural Network with Gated
145 Recurrent Units cell (RNN-GRU).

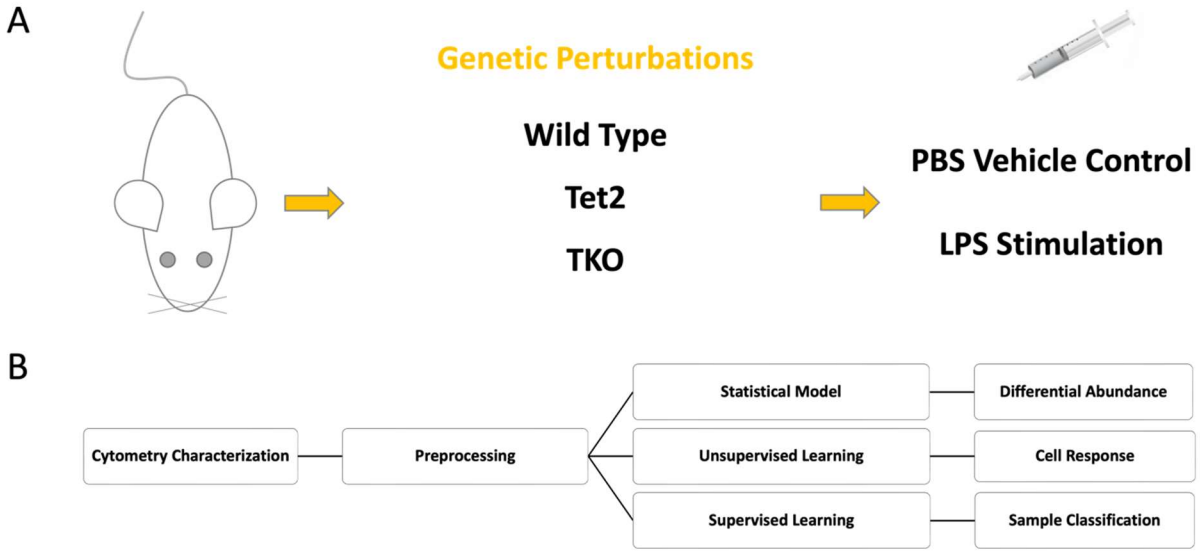

Figure 1. MDL4Cyto pipeline for analysis of single-cell mass cytometry data. Bone marrow samples (**A**) were harvested from genetically perturbed murine models (Wild Type [WT], *VavCreBaxBakBid* triple-knockout [TKO], and *VavCreTet2* knock-out [Tet2 KO]), which had been treated with LPS stimulation or PBS vehicle control. Statistical, unsupervised, and supervised learning models were implemented in our *Mechanistic Deep Learning for Cytometry* (MDL4Cyto) framework. The analysis pipeline **(B)** was benchmarked, using the reference dataset obtained from mass cytometry characterization, for the tasks of differential abundance analysis, cell response detection, and sample type classification.

Statistical modeling of genetically-determined or condition-dependent effects

The cell count summary statistic, which was calculated on the reference dataset, was found to be altered by genetic perturbations and/or LPS stimulation (Figure S1). Clear differences were observed for all markers. As reported in our previous work[14] and other studies[19], the TKO sample leads to necrosis with increasing production of cytokines. Enhanced inflammatory signaling was also observed in Tet2-deficient samples, as has also been previously described[19]. We observed a statistically significant difference in cell count for Sca1 (LSK cells), CD45 (leukocyte), TNFα (cytokines), and Caspase 3 (cell

163 death indicator) with respect to genetic perturbation (Figure 2A). Markers of cytokines were found to be

164 highly correlated with other surface markers, especially under LPS stimulation (Figure 2B).

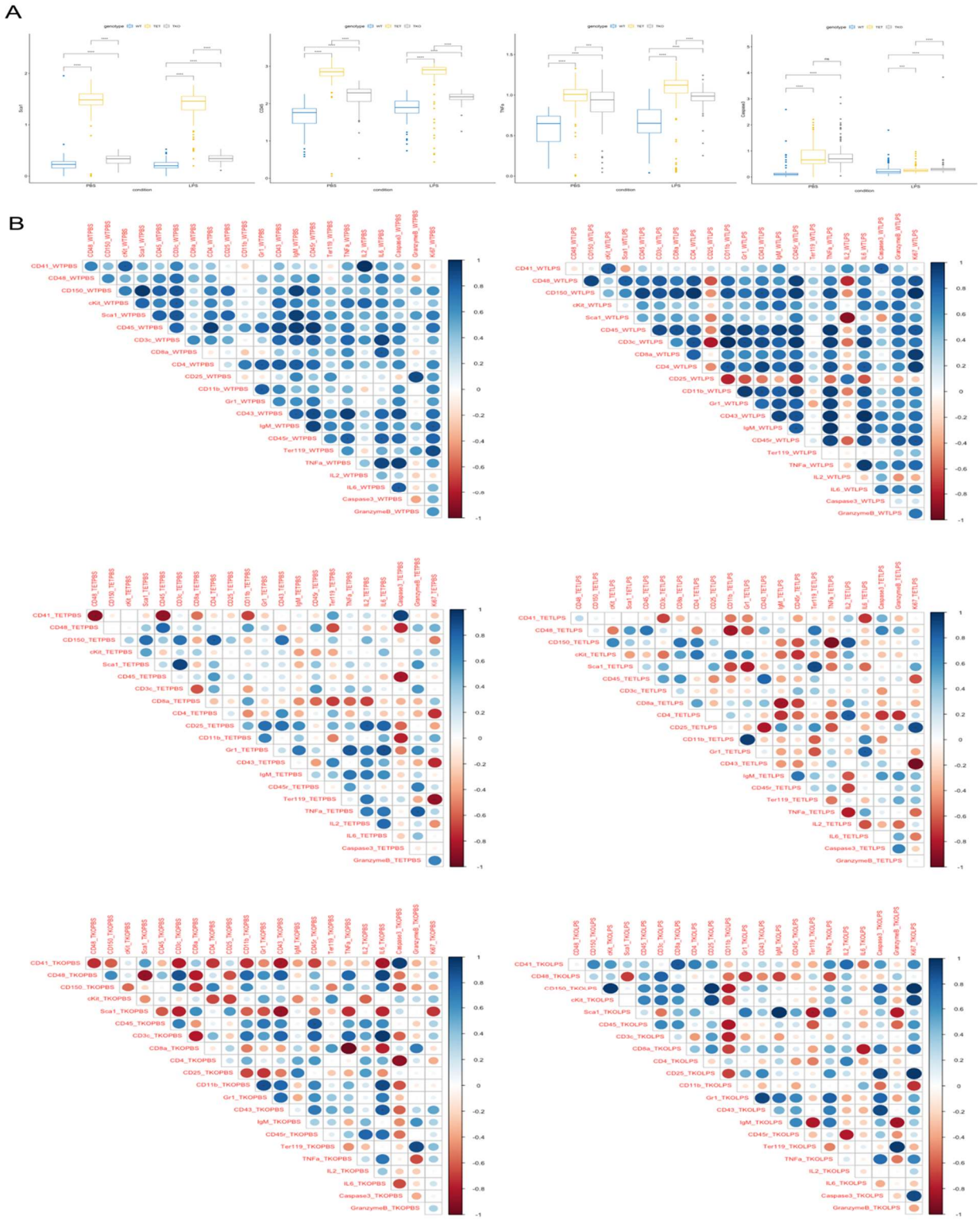

Figure 2. Impact of genetic perturbations on cell populations and correlations among the markers. A statistically significant change in cell count was observed for Sca1 (LSK cells), CD45 (leukocyte), cytokines

168 (TNFα), and Caspase 3 and (cell death indicator) in both the PBS vehicle control and LPS stimulation
169 condition, demonstrating genetic perturbations altering cell subpopulations **(A)**. Cytokines from genetic
170 knock-out samples were highly correlated with other surface markers, in particular under LPS
171 stimulation **(B)**, which is consistent with the biological context. (Wilcoxon test was performed for the
172 pairwise comparisons; Pearson correlation was calculated for the markers along with 95% confidence
173 interval. *p<.05, **p<0.01, ***p<0.001, ****p<0.0001).

174

175 The data profiles obtained from cytometry characterizations are dynamical panels, i.e., have a
176 time component. To estimate the overall effects of genotype and condition, we analyzed the
177 progression of marker Intensity for Ki67 from the aggregated data panel with 1 hour binning window
178 (Figure 3 and **Methods**). Ki67 is a proliferation protein that is increased in the S phase of the cell cycle
179 and indicates proliferating cells. We observed progression divergence according to genotype (Figure 3A)
180 and differentiated marker intensity between conditions (PBS vs LPS, Figure 3B). This is consistent with
181 our understanding that genetic perturbations and LPS stimulation impose pressures on differentiation
182 and cell cycle as dynamical processes. To achieve a better quantitative estimate of the contributions
183 arising from genotype and condition, we implemented GMM estimation. Besides the fixed and/or
184 interaction terms (**Methods**), the time term was considered in the model (Figure 3C). We applied
185 corrected Akaike's Information Criterion (AICc) and Bayesian Information Criterion (BIC) for model
186 evaluation and Marginal R squared (R2m) for variance coverage. Models built from genotype
187 demonstrated the best performance, which corroborates the fact that genetic perturbations have
188 significant impact on cellular differentiation and function. We note that the statistical modeling
189 implemented in MDL4Cyto (Figure 1B and **Methods**) is broadly applicable, which can facilitate the study
190 of cell fate decision and cell-type dynamics.

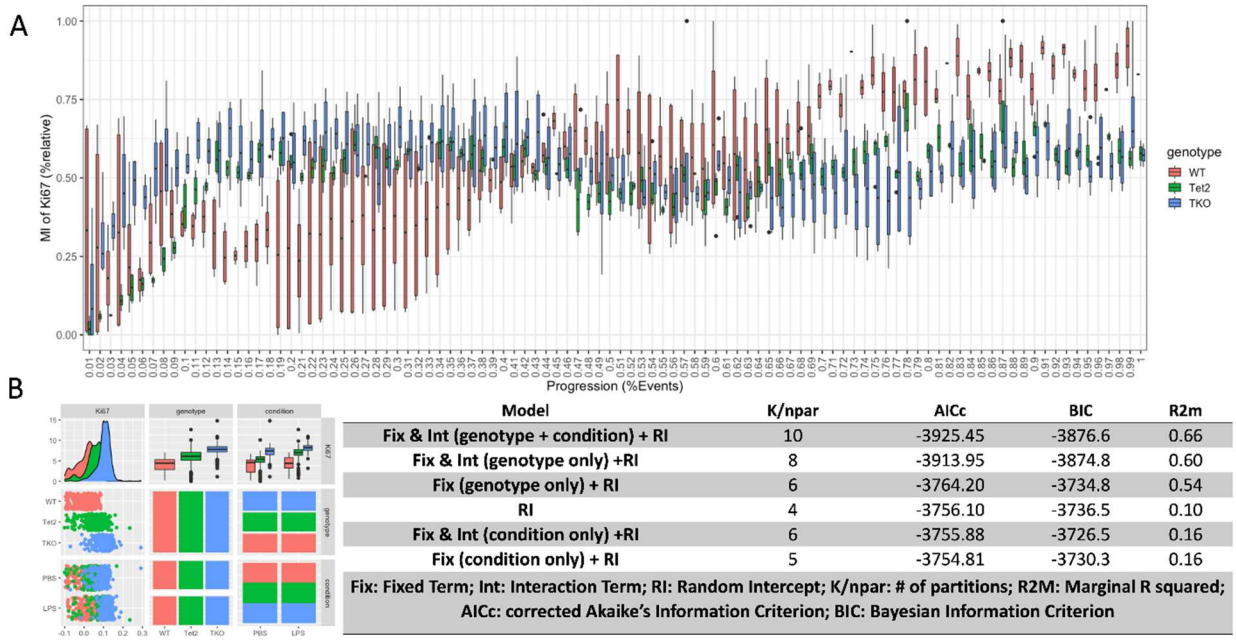

Model	K/npar	AICc	BIC	R2m
Fix & Int (genotype + condition) + RI	10	-3925.45	-3876.6	0.66
Fix & Int (genotype only) +RI	8	-3913.95	-3874.8	0.60
Fix (genotype only) + RI	6	-3764.20	-3734.8	0.54
RI	4	-3756.10	-3736.5	0.10
Fix & Int (condition only) +RI	6	-3755.88	-3726.5	0.16
Fix (condition only) + RI	5	-3754.81	-3730.3	0.16

Fix: Fixed Term; Int: Interaction Term; RI: Random Intercept; K/npar: # of partitions; R2M: Marginal R squared; AICc: corrected Akaike's Information Criterion; BIC: Bayesian Information Criterion

Figure 3. Analysis of dynamic data panel. Progression (%Events over the course of time) **(A)** and histogram **(B)** of cell count of proliferation marker Ki67 diverged with genetic background and shifted with condition. We implemented Generalized Mixed-Effects Model (GMM) estimation that considered the time term in addition to a fixed term and interaction term. While using genotype and condition as main parameters, several models were constructed, as represented by the equations in **(C)**. The performance of each model was further evaluated using the corrected Akaike's Information Criterion (AICc), Bayesian Information Criterion (BIC), and Marginal R squared (R2m). Genotype was identified as an important feature.

Quantifying cell response and population alteration via unsupervised learning

Identifying cell response from cell populations has been a key interest in mass cytometry analysis. Hematopoietic responses, induced either by genetic perturbations or by pathogen-like stimulation (LPS), were analyzed via pairwise comparisons, including WT-PBS vs TKO-PBS, WT-LPS vs TKO-LPS, WT-PBS vs Tet2-PBS, WT-LPS vs Tet2-LPS. Two established unsupervised learning algorithms, T-REX and PhenoGraph, were benchmarked in clustering our reference dataset (see Table S3 for the hyperparameters). Both algorithms apply k-nearest neighbors (kNN) for clustering and Uniform Manifold Approximation and Projection (UMAP) for dimension reduction and visualization. As illustrated in the UMAP plot, genetic perturbations induced alterations in cell subpopulations (Figure 4A&4B). Notably,

210 differential cell count of markers under a genetic perturbation, including Sca1, CD45, TNFα, and Caspase
211 3, could be seen in the mapping of cell count to the clusters (Figure S2, T-REX algorithm). These results
212 are consistent with the comparisons from our statistical tests (Figure 2A). Compared to conventional
213 methods, unsupervised learning showed a unique advantage in efficiently capturing changes in cell
214 populations. Cell subpopulations within the clusters were further investigated in two ways. While
215 reference datasets trained here contained only a single sample for each type, we created two pseudo-
216 replicates from a single sample (**Methods**) for the PhenoGraph algorithm, thus enabling differential
217 abundance analysis for the markers within each cluster (Figure 4C). On the other hand, populations from
218 the T-REX algorithm were screened and enriched through Density-Based Spatial Clustering and
219 Application with Noise (DBSCAN) and Marker Enrichment Modeling (MEM)[20] (Figure 4D). Strikingly, in
220 contrast to the T-REX method, our framework uncovered a strong signal from the cytokines, i.e., IL6 and
221 TNFα, from the differential abundance analysis (Figure 4C). This observation could well be attributed to
222 the known LPS-driven inflammation, as demonstrated by the enrichment analysis from MEM (Figure
223 4D). In addition, B cells and T cells are derived from the myeloid lineage, providing a broad and general
224 defense against foreign pathogens. Collectively, the TNFα and IL6 differential abundance results are
225 consistent with myeloid-driven or innate inflammation.

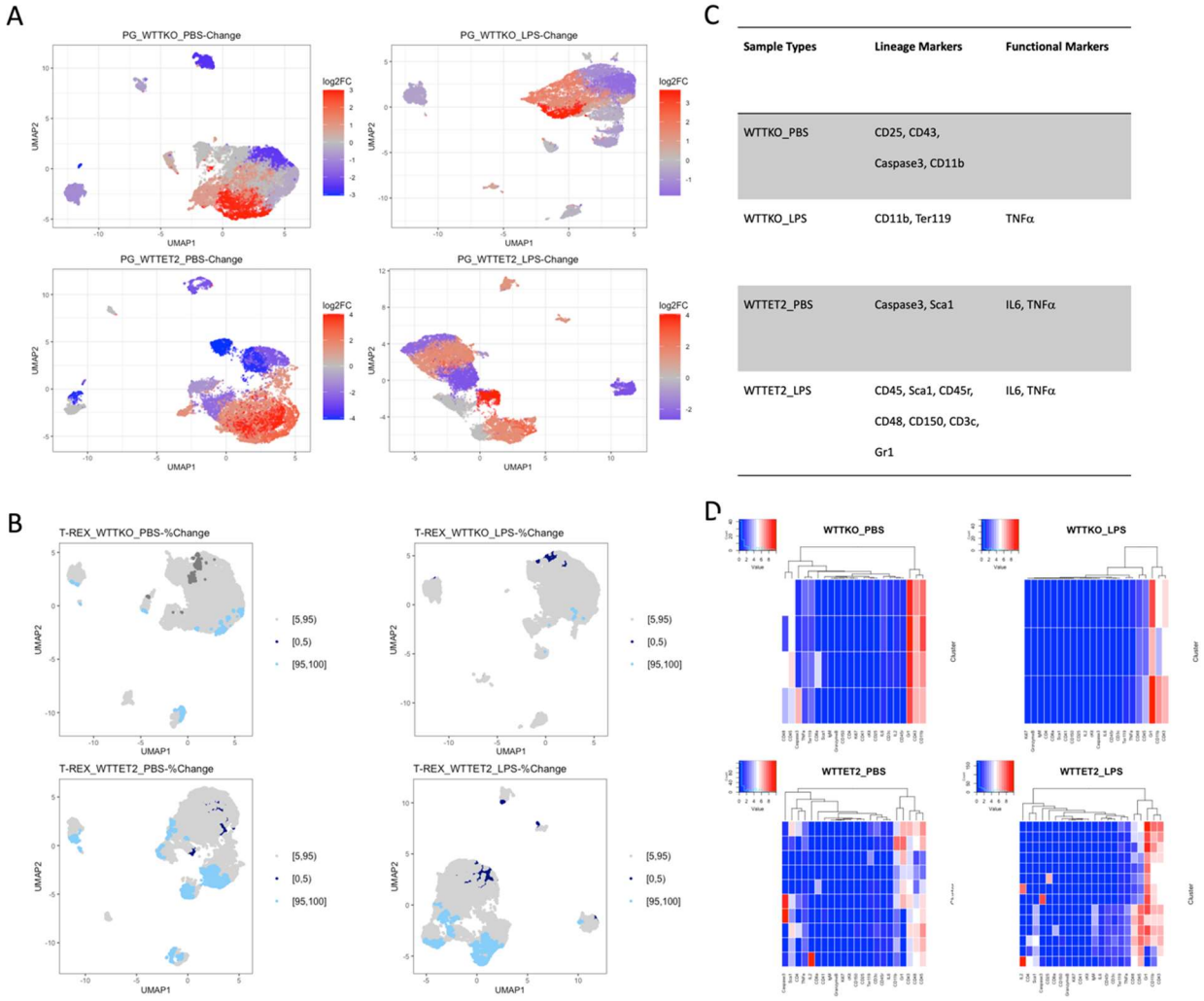

Sample Types	Lineage Markers	Functional Markers
WTTKO_PBS	CD25, CD43, Caspase3, CD11b	
WTTKO_LPS	CD11b, Ter119	TNFα
WTTET2_PBS	Caspase3, Sca1	IL6, TNFα
WTTET2_LPS	CD45, Sca1, CD45r, CD48, CD150, CD3c, Gr1	IL6, TNFα

Figure 4. Cell response identified by the unsupervised learning. Clustering from Phenograph **(A)** and T-REX **(B)** algorithms were performed on the paired genetically perturbed samples. PBS vehicle control and LPS stimulation were separately explored and compared. Using both algorithms, we found that the genetic perturbations altered the cell subpopulations. Clusters of significant fold changes identified from PhenoGraph were further explored for differential abundance of markers. Markers with significant responses that were captured in more than two clusters were identified **(C).** On the other hand, cell subpopulations obtained from T-REX were screened for those with significant changes and enriched through DBSCAN and MEM **(D)**.

Probing the regulatory cascade with biologically-informed neural networks

The hematopoietic system has classically been represented as a rigid hierarchical tree, illustrating HSC progression through multipotent, oligopotent, and bipotent stages. Evaluating a

239 “dynamic” model with complex interactions, we interrogated the marker/cell-type interactions within
240 the regulatory cascade from supervised learning models, considering both the network architecture and
241 prediction performance as probes. LPS stimulation impacts all stages of HSC differentiation, thus having
242 a global impact on all surface markers[18]. Therefore, we assigned PBS vehicle control and LPS stimulation
243 as predicted labels to the samples (**Methods**). Twenty-two lineage/functional makers from nine
244 different cell types (Table S1) were encoded as essential numerical features, while genotype was loaded
245 as an external categorical/global feature.

246 Considering each node as a marker/cell type, their interactions could be represented as network
247 connections. Specifically, a linear regression model reflects the additive effect from markers/cell types; a
248 dense neural network models the complex interactions among markers/cell types; and a tree model
249 considers the binary relations between levels within the hierarchy (Figure 5A). LPS stimulation on the
250 cells (the prediction label) could be treated as a perturbation on the neural network. In this model,
251 HSPCs will be differentiated to the common lymphoid progenitors, unipotent precursor cells as well as
252 megakaryocyte-erythroid progenitor cells, eventually producing mature cells. Informed by the
253 differentiation hierarchy, we implemented Boosted Tree (BT) and Random Forest (RF) models along with
254 two reference models, Linear Regression (LR) and Deep Neural Network (DNN). The four models varied
255 in performance: Linear Regression (LR) achieved a prediction accuracy of 64.8%; the DNN model with
256 three-hidden layers enhanced the accuracy to 68.1%; the Boosted Tree (BT) model further increased the
257 prediction performance to 72.7%; and the Random Forest (RF) models topped the accuracy at 77.13%
258 (Figure 5B). This overall pattern of prediction accuracy (LR < DNN < BT < RF) suggests a non-linear,
259 hierarchical relationship among the features, consistent with the classical hematopoietic hierarchical
260 tree. Interestingly, when we stacked a Deep Neural Network on top of the Random Forest model, where
261 DNN functioned as a denoising head[21], the new stacked model showed degraded performance in
262 comparison to the RF model alone.

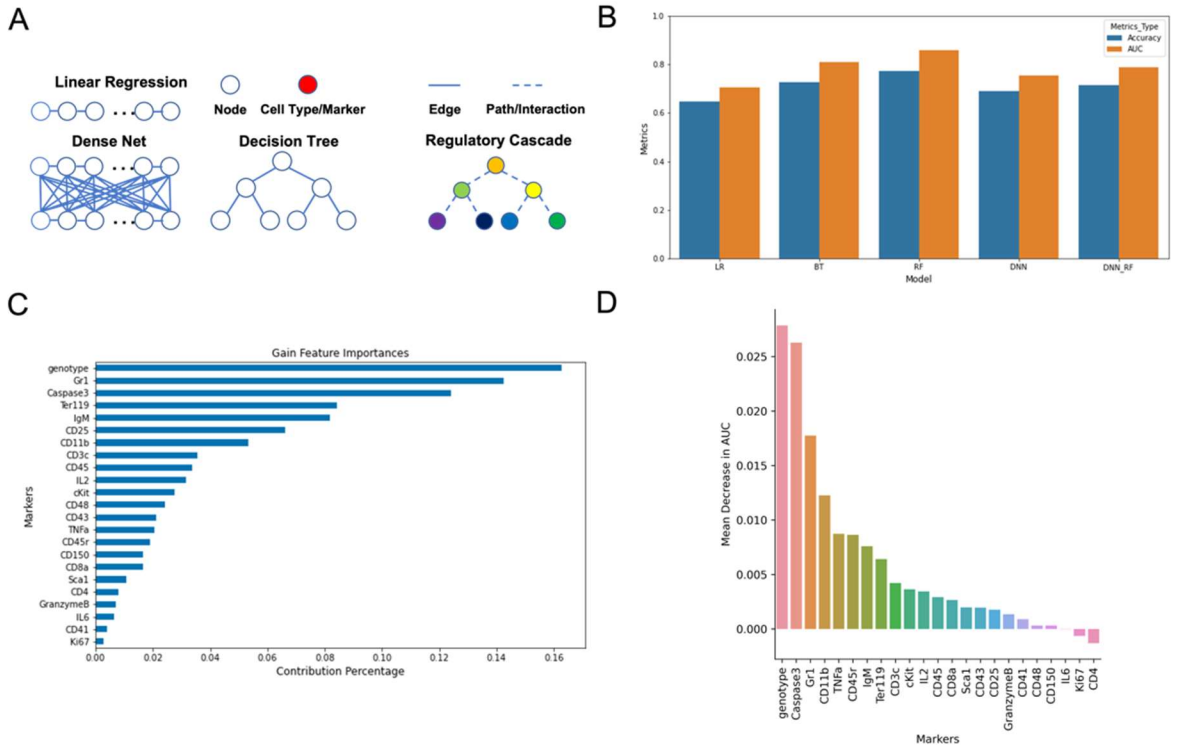

Figure 5. Mechanistic insights extracted from biologically-informed neural networks. Our neural network designs were guided by the biological context, in which we considered each node as a marker. The marker/cell-type interactions could therefore be represented as a network **(A)**, e.g., a decision tree or neural network could be linked to the regulatory cascade. With PBS vehicle control and LPS stimulation as labels, tree-based models (Boosted Tree [BT] and Random Forest [RF]) showed improved performance compared to Linear Regression (LR) and Deep Neural Network (DNN) models as well as DNN-RF stacked models **(B),** consistent with the hematopoietic tree hierarchy (i.e., representing a sequential binary branching decision process) among the markers. Feature importance of individual markers in the BT model, which implements gain-based feature importance **(C),** and RF model, which implements mean decrease in AUC **(D),** were examined. The group of markers with significant contributions would imply an overall cell response under inflammatory (LPS), e.g., pathogen-induced, challenges.

We further considered the feature contributions of individual markers using gain-based feature importance (Figure 5C) and mean decrease in AUC (Figure 5D). Gain-based feature importance reflects the relative contribution of a given feature to the model. Mean decrease in AUC indicates the decline in performance once the corresponding feature has been removed from the training dataset. We hypothesized that markers/features with the top feature contributions are biologically meaningful.

282 Indeed, the single most important contribution came from the strongest perturbation – genotype.
283 Individual markers, including Caspase3, Gr1, IgM, CD11b, and CD25, that contribute substantially to the
284 prediction of LPS stimulation, are highly biologically relevant in the full differentiation cycle of
285 hematopoiesis. Caspase 3 is an important player in the regulated cell death. Gr1 and CD11b reflect a
286 response from myeloid cells. And Ter119 indicates a strong immune response from the erythrocytes
287 under inflammatory challenges.

288

289 **Applying machine learning in sample classification**

290 While conventional methods/pipelines are limited by domain knowledge or manual
291 intervention, a predictive model that bypasses cell clustering or manual gating may provide an end-to-
292 end approach to the analysis of mass cytometry data. Here, we benchmarked a group of supervised
293 learning models, including CNN-1D, CNN-2D, RNN-LSTM, and RNN-GRU, that directly handle the raw
294 cytometry profiles for sample classification, i.e., prediction of clinical or biological outcome (Figure 6A).
295 We established multi-class output labels corresponding to six different sample types, including WT-PBS,
296 WT-LPS, Tet2-PBS, Tet2-LPS, TKO-PBS, and TKO-LPS. We used the curated ensemble of (1 hour)
297 "segments" from the initial bulk samples in evaluating the model performance. We found that CNN and
298 RNN-derived models demonstrated good prediction performance with at least 95% accuracy (Figure 6B).
299 We argue that convolutional layers and recurrent cells are efficient in learning the relevant features.
300 Algorithms such as CNN and LSTM as applied here, with cell count as the trait, captured with greater
301 fidelity the landscape of marker/cell-type interactions than the tree-based discrete models evaluated
302 above.

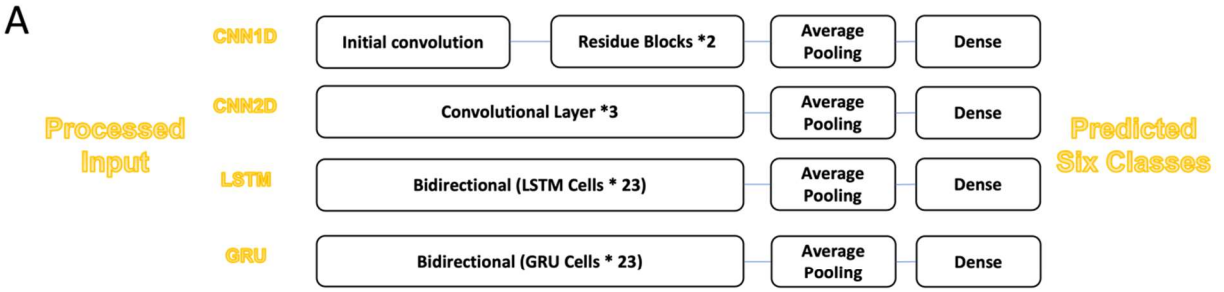

B

Model	Train Acc	Val Acc	Test Acc
CNN-1D	0.99783	0.97400	0.95887
CNN-2D	0.97580	0.95233	0.96537
RNN-LSTM	0.99819	0.96425	0.97186
RNN-GRU	1.000	0.98375	0.98052

Figure 6. Supervised learning identified sample type with high prediction performance. Convolutional Neural Network (CNN) and Recurrent Neural Network (RNN) derived models (CNN-1D, CNN-2D, RNN-LSTM, RNN-GRU) were benchmarked for the task of sample type classification. The specifics of the architectures are shown in **(A)**. All tested models achieved high performance with over 95% in accuracy **(B),** demonstrating the importance of learning the complex interactions and high-order features.

Discussion

The current single-cell genomic revolution has enabled entire systems, such as the hematopoietic system, to be interrogated comprehensively at an unprecedented resolution, revealing a previously unappreciated degree of functional and phenotypic variation within cell compartments. In this work, bone marrow samples were harvested from mice and further characterized in mass cytometry – the baseline murine model (WT) was compared to genetic perturbations, including *Tet2*-knockout (*VavCreTet2*) and *VavCreBaxBakBid* triple-knockout (TKO). LPS served as an external stimulus or an innate immune response, simulating pathogen infection. Statistical modeling and unsupervised learning revealed the direct effect of genetic perturbations. Markers of interest that are typically processed individually could be combined in unsupervised learning models. Importantly, we revealed a close connection among the intrinsic hierarchy of HSPC differentiation, neural network architecture, and prediction performance. Specifically, Boosted Tree (BT) and Random Forest (RF), which closely resemble

322 the stepwise binary branching decisions of the classical hierarchical model of hematopoiesis, showed
323 superior performance in comparison with Linear Regression (LR), Deep Neural Network (DNN) or even
324 the DNN-RF stacked model. The prediction performance was substantially enhanced relative to neural
325 network models, as the model reflected the cell differentiation cascade. However, as recent studies with
326 functional assays, non-invasive lineage tracing, and omics studies at single-cell resolution have shown[22],
327 hematopoiesis is a continuous process in which obvious boundaries are lacking between cell populations
328 located at different levels of the hierarchy. Consequently, given their architecture, tree-based models
329 may have an inherent limitation in capturing transition states, even with extensive optimization,
330 constraining their ability to further improve prediction performance. From this perspective, the complex
331 relationships among the cell populations (including feed-back loops in pathways) may be better
332 elucidated by neural networks.

333 Nevertheless, results of the analyses from the machine learning models were consistent with
334 biological insights such as myeloid-driven or innate inflammation (responses from TNFα and IL6). In
335 summary, the presented framework provides a unifying methodological framework for the analysis of
336 cytometry data, combining data-driven and model-driven approaches. We constructed interpretable
337 models that are anchored in biological context, with implications for ongoing and future studies in
338 single-cell biology.

339

340 Limitations of the study

341 Machine learning models, including graphical representation learning and tree-based
342 algorithms, were trained in datasets obtained from mass cytometry (CyTOF) characterization. While we
343 designed the neural network architectures with biological information as guide, assumptions of cell
344 types as nodes and edges as their interactions within a graph-based framework are based on the classic

discrete cell differentiation model. Cell differentiation is a continuous process, with intermediate states among various levels leading to much more complex networks.

Methods

Mass cytometry and murine samples

Three generic murine models were included in this study, namely, wild type (WT), Tet2 knockout (Tet2)[23], and *VavCreBaxBakBid* triple-knockout (TKO)[14]. Prior to bone marrow isolation, the mice had been treated with LPS or PBS. The obtained samples for the six genotype-condition types were subsequently characterized using mass cytometry, according to previously established protocols[24]. Specifically, mass cytometry staining was performed on whole bone marrow with antibodies conjugated to heavy metals. Cell responses from 9 different cell type and functional categories (stem cells, pan leukocyte, T lymphocytes cells, mature myeloid cells, B cells, erythrocytes, cytokines, cell death and proliferation) were recapitulated by 16 surface/lineage markers and 6 function/intracellular markers. Markers from pre-gating channels (DNA-1 and DNA-2) and instrument channels (Time/Event) were also considered (Table S1). The CyTOF data generated from the six samples consisted of a maximum of 293,778 cells and a minimum of 121,124 cells.

Data pre-processing

Initial cell count data profiles obtained from the mass cytometry characterization were filtered out for debris, doublets, and dead cells, thus reducing noise. They are represented as dynamical panels on which the *arcsinh* transformation with co-factor = 5 and a binning window of 30 seconds was applied. We sought to analyze the data in a way that maximizes robustness. The processed profiles were sliced into ensembles of “segments” to achieve an optimized tradeoff between computational efficiency and prediction accuracy. We evaluated an array of sizes ([2, 10, 30, 60, 120, 240, 480]), corresponding to

368 2*30S=1M, 10 * 30S = 5M, 30 * 30S = 15M, 120 * 30S = 1H, 240 * 30S = 2H, & 480 * 30S = 4H sampling
369 intervals (M: Minute, H: Hour), respectively. The obtained pile of "segments" was completely shuffled
370 and re-assembled into new ensembles. We implemented an RNN-LSTM model for this special
371 "hyperparameter search" (see prediction accuracy in Table S2) to determine the optimal segment size,
372 which was 1H. Signals of select markers, including Sca1, CD45, TNFα, Caspase 3, and Ki67, were
373 aggregated and averaged into 1 hour binning window for the statistical test and GMM estimation.

374 **Mechanistic Deep Learning Framework**

375 *Statistical test and model*

376 Wilcoxon test was performed on pairwise comparisons of marker intensity. Pearson correlation
377 coefficient was calculated for inter-marker association. We implemented a GMM on the marker Ki67.
378 We considered fixed effects and interactions among time, genotype, and condition (PBS control or LPS
379 stimulation). After testing the random slope of a sample, $(1 + \text{Time} \mid \text{Sample})$, we considered only the
380 random intercept from a sample, i.e., $(1 \mid \text{Sample})$. The models were evaluated using corrected Akaike's
381 Information Criterion (AICc), Bayesian Information Criterion (BIC), and Marginal R squared (R2M). The
382 optimal model was found to be given by the following expression:

383 $$\text{Marker Intensity} = \text{Time} + \text{Genotype} + \text{Condition} + \text{Genotype:Time} + \text{Condition:Time} + (1 \mid \text{Sample}) + \varepsilon$$

384 *Unsupervised Learning models*

385 We analyzed two established unsupervised learning pipelines, namely Phenograph[5] and T-REX[6],
386 which were applied to the preprocessed CyTOF dataset with binning window 30S. For both pipelines,
387 Uniform Manifold Approximation and Projection (UMAP)[25] was used for dimensionality reduction; k-
388 nearest neighbors (kNN)[26] for clustering; Marker Enrichment Modeling (MEM) for generating the
389 enriched heatmap. The applied hyper-parameters are presented in Table S3. For comparison, we

390 screened and enriched the cell populations derived from the T-REX algorithm through Density-Based
391 Spatial Clustering and Application with Noise (DBSCAN) and MEM.

392 *Supervised Learning models*

393 All the machine learning models were trained using the *TensorFlow (TF)* ecosystem[27], which we
394 applied to the preprocessed CyTOF dataset (with binning window size of 30S) to perform model training
395 and evaluation. Linear Regression (LR), Deep Neural Network (DNN), Boosted Tree (BT) and Random
396 Forest (RF) models were implemented on the dataset with train and test split of 8:2. A stacked model of
397 Dense Neural Network and Random Forest (DNN-RF) was constructed following the same splitting.
398 Models implementing a Convolutional Neural Network (CNN) or a Recurrent Neural Network (RNN) in
399 the framework include CNN-1D, CNN-2D, RNN-LSTM, and RNN-GRU. For these four architectures, pre-
400 processed datasets were divided into train, valid, and test data according to 6:2:2 ratio.

401

402 **Acknowledgments**

403 This research is supported by National Institutes of Health (NIH) grants NHGRI R35HG010718,
404 NHGRI R01HG011138, NIA AG068026, and NHLBI R01HL133559.

405

406 **Author contributions**

407 B.W., S.S.Z., and E.R.G. conceived the project and designed the study. B.W. performed the
408 analyses and drafted the article. B.W., S.S.Z., and E.R.G. revised the article. S.S.Z. and E.R.G. supervised
409 the project and acquired funding for the study.

410

411

412

413 **References**

414 1. Davis, M. M., Tato, C. M. & Furman, D. Systems immunology: just getting started. *Nat. Immunol.* **18**,

415 725–732 (2017).

416 2. Gadalla, R. *et al.* Validation of CyTOF Against Flow Cytometry for Immunological Studies and

417 Monitoring of Human Cancer Clinical Trials. *Front. Oncol.* **9**, (2019).

418 3. Bendall, S. C. *et al.* Single-Cell Mass Cytometry of Differential Immune and Drug Responses Across a

419 Human Hematopoietic Continuum. *Science* **332**, 687–696 (2011).

420 4. Hahne, F. *et al.* flowCore: a Bioconductor package for high throughput flow cytometry. *BMC*

421 *Bioinformatics* **10**, 106 (2009).

422 5. Levine, J. H. *et al.* Data-Driven Phenotypic Dissection of AML Reveals Progenitor-like Cells that

423 Correlate with Prognosis. *Cell* **162**, 184–197 (2015).

424 6. Barone, S. M. *et al.* Unsupervised machine learning reveals key immune cell subsets in COVID-19,

425 rhinovirus infection, and cancer therapy. *eLife* **10**, e64653 (2021).

426 7. Hu, Z., Tang, A., Singh, J., Bhattacharya, S. & Butte, A. J. A robust and interpretable end-to-end deep

427 learning model for cytometry data. *Proc. Natl. Acad. Sci.* **117**, 21373–21380 (2020).

428 8. Arvaniti, E. & Claassen, M. Sensitive detection of rare disease-associated cell subsets via

429 representation learning. *Nat. Commun.* **8**, 14825 (2017).

430 9. Liggett, L. A. & Sankaran, V. G. Unraveling Hematopoiesis through the Lens of Genomics. *Cell* **182**,

431 1384–1400 (2020).

432 10. Domen, J., Cheshier, S. H. & Weissman, I. L. The role of apoptosis in the regulation of

433 hematopoietic stem cells: Overexpression of Bcl-2 increases both their number and repopulation

434 potential. *J. Exp. Med.* **191**, 253–264 (2000).

435 11. Kale, J., Osterlund, E. J. & Andrews, D. W. BCL-2 family proteins: changing partners in the dance
436 towards death. *Cell Death Differ.* **25**, 65–80 (2018).
437 12. Salisbury-Ruf, C. T. *et al.* Bid maintains mitochondrial cristae structure and function and protects
438 against cardiac disease in an integrative genomics study. *eLife* **7**, e40907 (2018).
439 13. Gamazon, E. R. *et al.* A gene-based association method for mapping traits using reference
440 transcriptome data. *Nat. Genet.* **47**, 1091–1098 (2015).
441 14. Wagner, P. N. *et al.* Increased Ripk1-mediated bone marrow necroptosis leads to myelodysplasia
442 and bone marrow failure in mice. *Blood* **133**, 107–120 (2019).
443 15. Lun, A. T. L., Richard, A. C. & Marioni, J. C. Testing for differential abundance in mass cytometry
444 data. *Nat. Methods* **14**, 707–709 (2017).
445 16. Wang, B. & Gamazon, E. R. *Towards mechanistic models of mutational effects: Deep Learning on*
446 *Alzheimer's Aβ peptide*. 2021.12.19.473403
447 https://www.biorxiv.org/content/10.1101/2021.12.19.473403v2 (2021)
448 doi:10.1101/2021.12.19.473403.
449 17. Wang, B. & Gamazon, E. R. Modeling mutational effects on biochemical phenotypes using
450 convolutional neural networks: application to SARS-CoV-2. *bioRxiv* 2021.01.28.428521 (2021)
451 doi:10.1101/2021.01.28.428521.
452 18. King, K. Y. & Goodell, M. A. Inflammatory modulation of HSCs: viewing the HSC as a foundation
453 for the immune response. *Nat. Rev. Immunol.* **11**, 685–692 (2011).
454 19. Cai, Z. *et al.* Inhibition of Inflammatory Signaling in Tet2 Mutant Preleukemic Cells Mitigates
455 Stress-Induced Abnormalities and Clonal Hematopoiesis. *Cell Stem Cell* **23**, 833-849.e5 (2018).
456 20. Diggins, K. E., Greenplate, A. R., Leelatian, N., Wogsland, C. E. & Irish, J. M. Characterizing cell
457 subsets using marker enrichment modeling. *Nat. Methods* **14**, 275–278 (2017).

458 21. Xie, J., Xu, L. & Chen, E. Image Denoising and Inpainting with Deep Neural Networks. in *Advances*
459 *in Neural Information Processing Systems* vol. 25 (Curran Associates, Inc., 2012).
460 22. Zhang, Y., Gao, S., Xia, J. & Liu, F. Hematopoietic Hierarchy – An Updated Roadmap. *Trends Cell*
461 *Biol.* **28**, 976–986 (2018).
462 23. Moran-Crusio, K. *et al.* Tet2 loss leads to increased hematopoietic stem cell self-renewal and
463 myeloid transformation. *Cancer Cell* **20**, 11–24 (2011).
464 24. Zinkel, S. S. *et al.* Proapoptotic BID is required for myeloid homeostasis and tumor suppression.
465 *Genes Dev.* **17**, 229–239 (2003).
466 25. McInnes, L., Healy, J. & Melville, J. UMAP: Uniform Manifold Approximation and Projection for
467 Dimension Reduction. *ArXiv180203426 Cs Stat* (2020).
468 26. Mucherino, A., Papajorgji, P. J. & Pardalos, P. M. k-Nearest Neighbor Classification. in *Data*
469 *Mining in Agriculture* (eds. Mucherino, A., Papajorgji, P. J. & Pardalos, P. M.) 83–106 (Springer, 2009).
470 doi:10.1007/978-0-387-88615-2_4.
471 27. Abadi, M. *et al.* TensorFlow: Large-Scale Machine Learning on Heterogeneous Distributed
472 Systems. 19.
473
474
475
476
477
478
479
480

481

482 # Supplementary Information

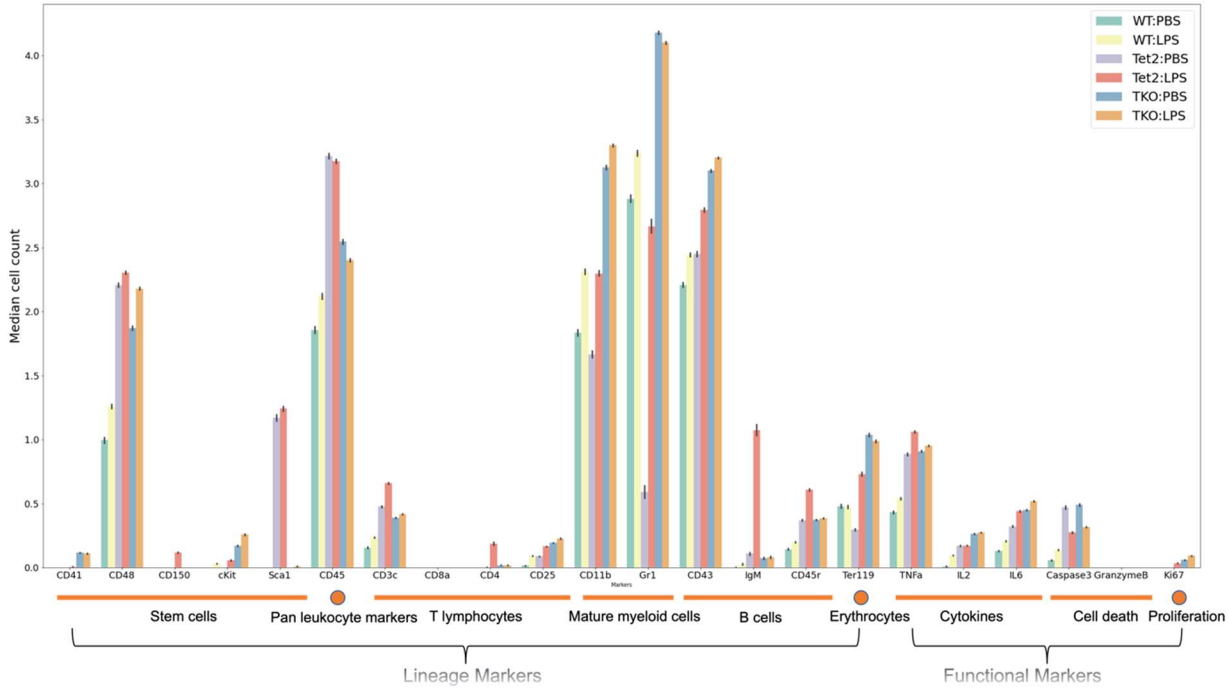

483

484 **Figure S1. Summary statistics on the cell count.** Initial sample data profiles (WT-PBS, WT-LPS, Tet2-PBS,

485 Tet2-LPS, TKO-PBS, and TKO-LPS) were obtained from mass cytometry characterization, where summary

486 statistics on the transferred cell count were computed. Lineage and functional markers are grouped

487 based on cell type.

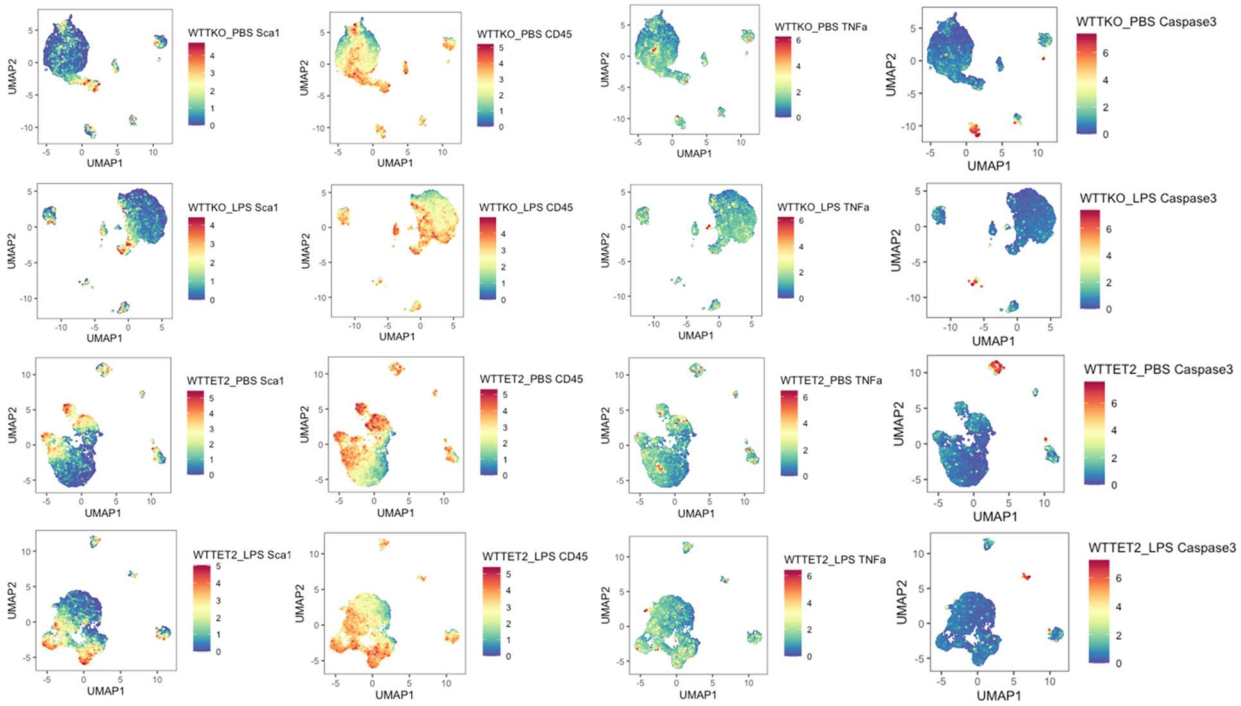

488

489 **Figure S2. Differential cell count illustrated from the unsupervised learning.** Markers of interest under

490 genetic perturbation, including Sca1 (LSK cells), CD45 (Leukocyte), TNFα (Cytokines) and Caspase 3 (Cell

491 Death Indicator), were mapped to the clustering results from the T-REX algorithm.

492

493 **Table S1.** Cell markers investigated in this study

Marker Type	Cell Type	Marker Names
Lineage	Stem Cells	CD41, CD48, CD150, cKit, Sca1
Lineage	Pan Leukocyte	CD45
Lineage	T Lymphocytes	CD3c, CD8a, CD4, CD25
Lineage	Mature Myeloid	CD11b, Gr1
Lineage	B Cells	CD43, IgM, CD45R
Lineage	Erythrocytes	Ter119

Functional	Cytokines	TNF alpha, IL2, IL6
Functional	Cell Death	Caspase3, Granzyme B
Functional	Proliferation	Ki67
Pre-gating		DNA1, DNA2
Instrument		Cell Length, Time

494

495 **Table S2**. Searching for the optimal size "hyperparameter" via RNN-LSTM model architecture

Micro Sample Size	Train Acc	Val Acc	Test Acc
2	0.73653	0.71342	0.71033
10	0.93403	0.88667	0.87375
30	0.99791	0.95369	0.95125
60	**0.99499**	**0.9325**	**0.9575**
120	1.0	0.9598	0.975
240	1.0	0.93	0.93
480	1.0	0.77551	0.88

496

497 **Table S3.** Hyperparameters applied in PhenoGraph and T-REX

Key components in pipeline	Phenograph	T-REX
UMAP	ret_nn = TRUE	
kNN	k = 30 for single sample, k = 60 for paired sample	

498